Int. J. Electrochem. Sci., 12 **(2017)** 6520 – 6534, doi: 10.20964/2017.07.48

International Journal of
ELECTROCHEMICAL
SCIENCE
www.electrochemsci.org

Effects of stray AC on delamination of epoxy coatings with defects in 3.5% NaCl solution

Xinhua Wang, Cheng Xu, Qiang Liu, Chengyuan Tu, Yingchun Chen, Yingchao Li[*],

College of Mechanical Engineering and Applied Electronics Technology, Beijing University of Technology, 100 Ping Le Yuan, Chaoyang District, Beijing 100124, China
[*]E-mail: liyc@bjut.edu.cn

Received: 8 March 2017 / *Accepted:* 11 April 2017 / *Published:* 12 June 2017

The stray current induced coating delamination at defect areas is complicated and with its mechanism uncovered. In this study, the delamination mechanism of epoxy coating at defect areas under stray alternating current (AC) interference was investigated using electrochemical methods and software simulation. The simulation results indicated that stray AC at defect areas was not evenly distributed. The current density at the defect edge was higher than that at the defect center. The electrochemical results showed different electrochemical behaviors on samples with a various size of defects as AC density increased. The impedance of samples with small defects decreased, on the contrary, the impedance of samples with large defects increased. The delamination area on samples with small defects was larger than that with large defects under the same level of AC interference. Furthermore, the AC interference resulted in a more severe corrosion damage at the small coating defects. Small defects deserve particular attention in the safety assessment at the presence of stray AC.

Keywords: Stray alternating current, coating defects, coating delamination, simulation

1. INTRODUCTION

In recent years, buried steel pipelines suffered from the increasing risk of stay alternating current (AC) interference due to the construction of high-voltage AC transmission lines and AC electrified railway. Stray current is defined as the current which deviates from the designed paths because of alternative routes with lower resistance [1–4]. It has been acknowledged that most metallic materials or structures corrode at an accelerated rate in the presence of a stray AC [5-9]. It was believed that a 100 A/m^2 stray AC is a threshold to judge the stray AC corrosion. In order to improve the integrity of buried pipelines, protective coatings and cathodic protection methods are usually

applied. However, due to the mechanical impact during installation and transportation, the stress among soil, pipeline, and coatings on the pipeline will inevitably produce some damage, scratches, pinholes and other defects. Soil corrosive media will permeate into the pipe surface along with the defects, forming the corrosion micro-environment, which will lead to serious corrosion damage to the pipelines [10,11]. The higher the resistance of the buried pipeline coating is, the greater the induced AC density at the coating defect. For instance, the pipes coated with 3PE, FBE, or other coatings with good resistance protected the pipelines from the threat of stray AC [12]. Forero et al. [13] discussed the problem of AC disturbed corrosion of buried pipelines near high-voltage transmission lines. It was believed that even in pipes with good coatings and cathodic protection system, the AC corrosion would still occur. The stray AC interference has become a new threat to the steel pipeline system in the oil and gas industry and other fields.

Stray current corrosion of high strength steel has been studied experimentally in the past few decades [14-17]. Up to now, there is no universal corrosion mechanism for AC corrosion, and scholars have proposed several theories to study stray AC corrosion. Li et al. [9] pointed out that the stray AC induced corrosion of high strength steel because the steel was in an anodic polarization status in most of the AC circle. It was found that the corrosion potential was shifted negatively by the stray AC. It is related to the ratio of the absolute value of the Tafel slope of the anode to the cathode [18,19]. Goidanich et al. [20] suggested that if the electrochemical process at the interface between iron and electric double layer was not completely reversible, the rectification effect of Faraday's Law was not able to explain the stray AC corrosion.

Generally, a protective coating must provide an adequate barrier to water, oxygen, and ions penetration to achieve a high resistance to delamination and blistering. Three types of coating failures are distinguished: osmotic blistering, cathodic delamination, and anodic undermining, in which the main failure type is delamination [21-23]. The pipeline materials at the damage areas directly contact with a corrosive medium in the environment, causing the occurrence of corrosion damage and the coating delamination [24-26]. Walkner and Hassel et al. [27] found that oxygen and water accumulated rapidly at the coating defects and started the cathodic polarization, which caused a high pH resulting in cathodic delamination. Stray AC corrosion belongs to localized corrosion and is likely to cause pits at coating defect areas. Additionally, stray AC potentially changed the micro-environment at the defect area, which is associated with coating delamination [28]. However, it has not been reported about the mechanism of stray AC promoting coating delamination and the critical current density of AC interference to cause coating delamination.

In this research, the delamination of epoxy coatings on X70 steel samples at defect areas was investigated using software simulation, electrochemical methods, and other advanced techniques. The distribution of stray current at the defect area was simulated using COMOSOL Multiphysics software. The electrochemical behavior and the delamination of the coating samples with defects were studied. The effect of the defect size on the coating delamination was obtained. The critical current density of the coating delamination under AC interference was determined by measuring the delamination area.

2. EXPERIMENTAL

2.1 Materials and samples

Table 1. Chemical composition of X70 pipeline steel (wt.%)

C	Si	Mn	P	Cu	Nb	Ni	Others
0.061	0.24	1.53	0.011	0.01	0.038	0.21	Fe

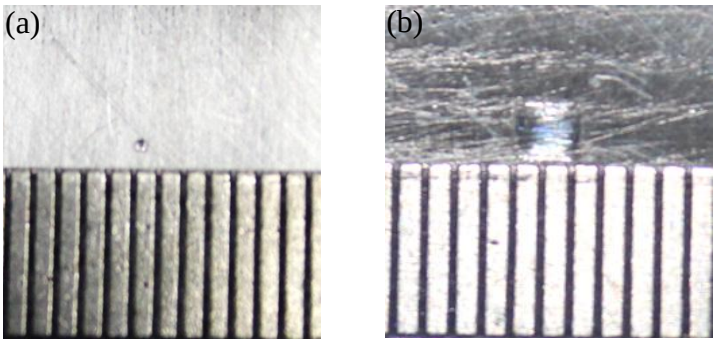

Figure 1. Artificial defects with different sizes (a) 0.5×0.5 mm^2, (b) 2×2 mm^2 on coating samples (the scale is 1 mm)

In this work, X70 high-strength pipeline steel was used. The chemical composition (wt.%) of X70 steel is shown in Table 1. The sample was machined by wire-cutting and the size was 40 mm × 40 mm × 2 mm. The sample surface was polished with finer SiC papers (60, 120, 400, 600 grit) subsequently. The surface of the sample was cleaned with acetone (analytical grade) and ethanol (analytical grade). The coating materials was an epoxy resin. Epoxy resin E51 and curing agent polyether amine d230 were evenly mixed with a mass ratio of 3:1 at room temperature (~25 ^oC). After brushing, the sample was placed in a drying oven and dried at 80 ^oC for 2 hours. The coating thickness was 60 ± 5μm. The copper wire was welded to the side of the specimen. As shown in Fig. 1, there are two kinds of spot defect (0.5×0.5 mm^2 and 2×2 mm^2) in the middle of the sample.

2.2 Electrochemical measurements

The electrochemical measurements were operated in 3.5% NaCl solution. The electrochemical setup and the stray current loading device were shown in Fig. 2. The electrochemical workstation was Solartron 1260/1287 (Hampshire, UK). Three electrode systems were used. The reference electrode was saturated calomel electrode (SCE), the counter electrode was a platinum electrode, and the working electrode was an X70 steel epoxy coating sample. The X70 steel epoxy coated samples and graphite electrodes were connected to an external AC signal generator (SG1005), respectively. In the AC signal external circuit, the capacitor (500 uF) was used to prevent the electrochemical workstation from the AC interfering. The inductance (15 H) was used to prevent the AC signal from direct current

interfering. In the experimental test, stray AC signals with different current densities (0 A/m^2, 30 A/m^2, 100 A/m^2, 300 A/m^2 and 500 A/m^2) were applied at a frequency of 50 Hz. The AC density was calculated based on the coating defect area. Open circuit potential (OCP) and electrochemical impedance spectroscopy (EIS) were measured after immersing 48 hours. Tests were performed at room temperature and all experimental results were repeated two times. In the EIS test, the amplitude of the excitation signal was 20 mV and the sweep frequency range was from 0.01 Hz to 10^6 Hz. EIS data were analyzed using ZSimpWin software.

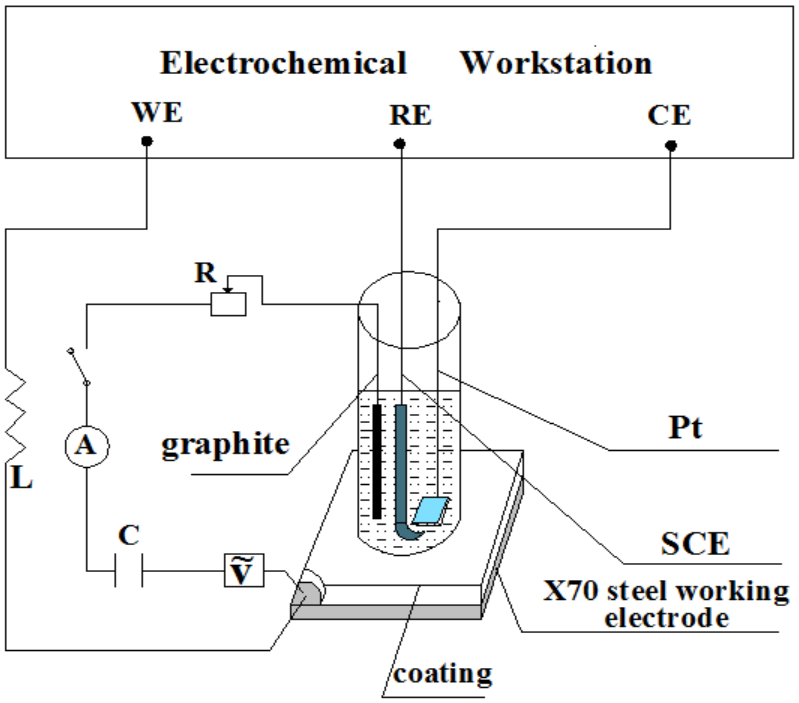

Figure 2. Electrochemical measurement and stray current loading setup

2.3 COMSOL Multiphysics simulation

Using COMSOL Multiphysics to study the transmission behavior of stray AC on the buried pipelines and the distribution at coating defect areas. The physical field selected the current module inside AC/DC, with the pipeline steel buried in the project model for three-dimensional modeling. Stray AC research was of the frequency domain. The external current was set to 300 A/m^2 with a frequency of 50 Hz.

3. RESULTS AND DISCUSSION

3.1 Simulation analysis

Fig. 3 is the AC distribution simulation result on the buried pipeline. In Fig. 3(a) to (d), the distribution of stray AC at the inner surface of the pipeline is not even and the current density is relatively small. The outer surface of the pipeline except for the defect area has a more uniform current distribution. The stray current is unevenly distributed at the defect area. The stray current density of

the defects edge is higher than the value in the defect center. The AC density at the coating defects is maximum, followed by the outer surface of the pipeline, the inner surface of the pipe is minimal. It is concluded that the coating defect areas were corroded severely under the stray current interference, it was very likely to cause pitting corrosion.

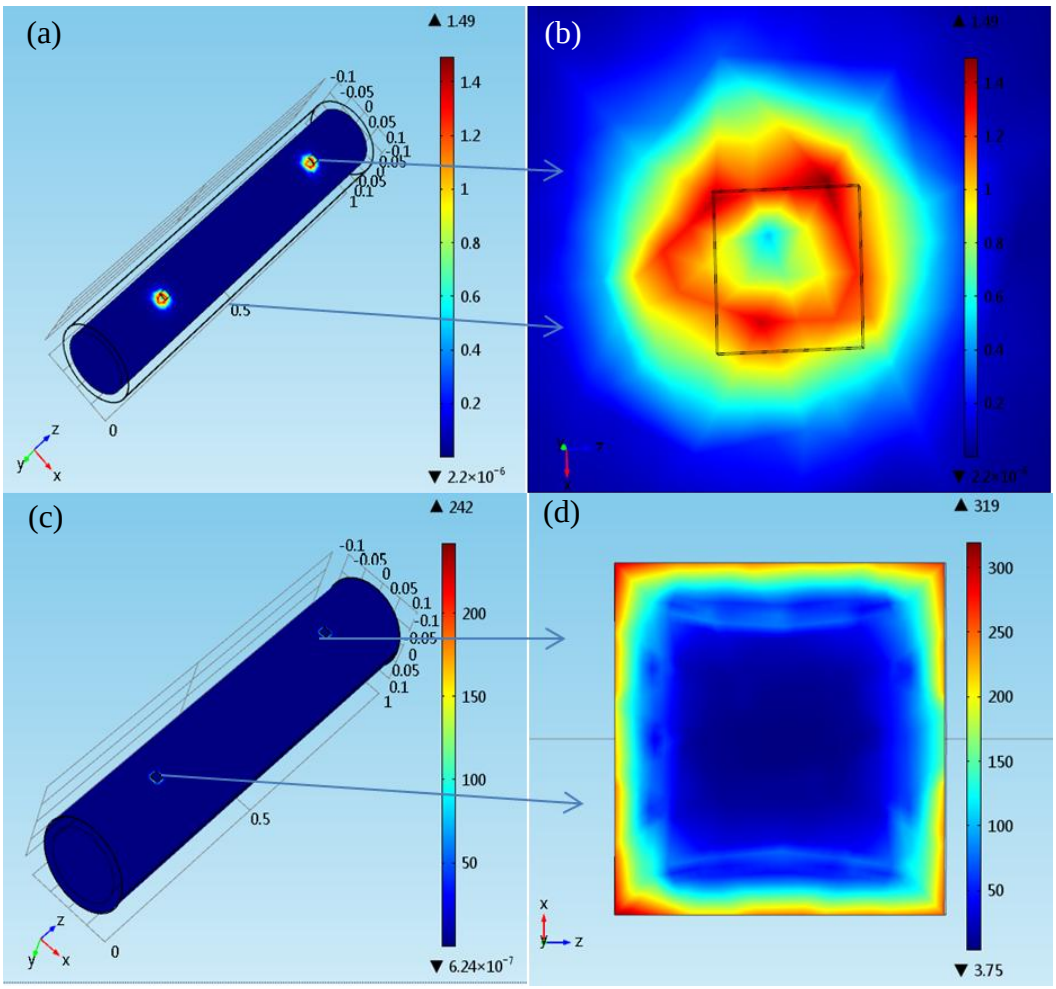

Figure 3. Simulation results of current densities(A/m^2) in different areas (a) the inner surface, (b) the enlarged view of the inner surface, (c) the outer surface, (d) the coating defects, of buried pipeline under stray AC interference

3.2 OCP analysis

Fig. 4 shows the open circuit potential (OCP) test results of X70 steel epoxy coating samples of different sizes under AC interference with various current densities. The OCP is negatively shifted with the increase of AC density. On the X70 steel epoxy coated sample with a defect area of 0.5×0.5 mm^2, the OCP is shifted from -0.619 V in the absence of AC interference to -0.638 V in the case of 30 A/m^2 AC interference. The OCP eventually shifts to -0.742 V with a 500 A/m^2 AC interference. On the coated sample with a defect area of 2×2 mm^2, the OCP is shifted from -0.635 V at no AC disturbance

to -0.645 V at 30 A/m^2 AC interference, The OCP eventually shifts to -0.7 V with a 500 A/m^2 AC interference. Obviously, the smaller the coating defect area of the coating is, the larger the negative shift of OCP is. When the coating defect area is 0.5×0.5 mm^2, the OCP of the final negative shift is 0.123 V. When the defect area is 2×2 mm^2, the OCP is eventually shifted with 0.06 V. The negative shift of OCP caused by stray AC would eventually increase the electrochemical activity on the steel surface from a thermodynamic perspective. Thus, the steel was more vulnerable to corrosion damage.

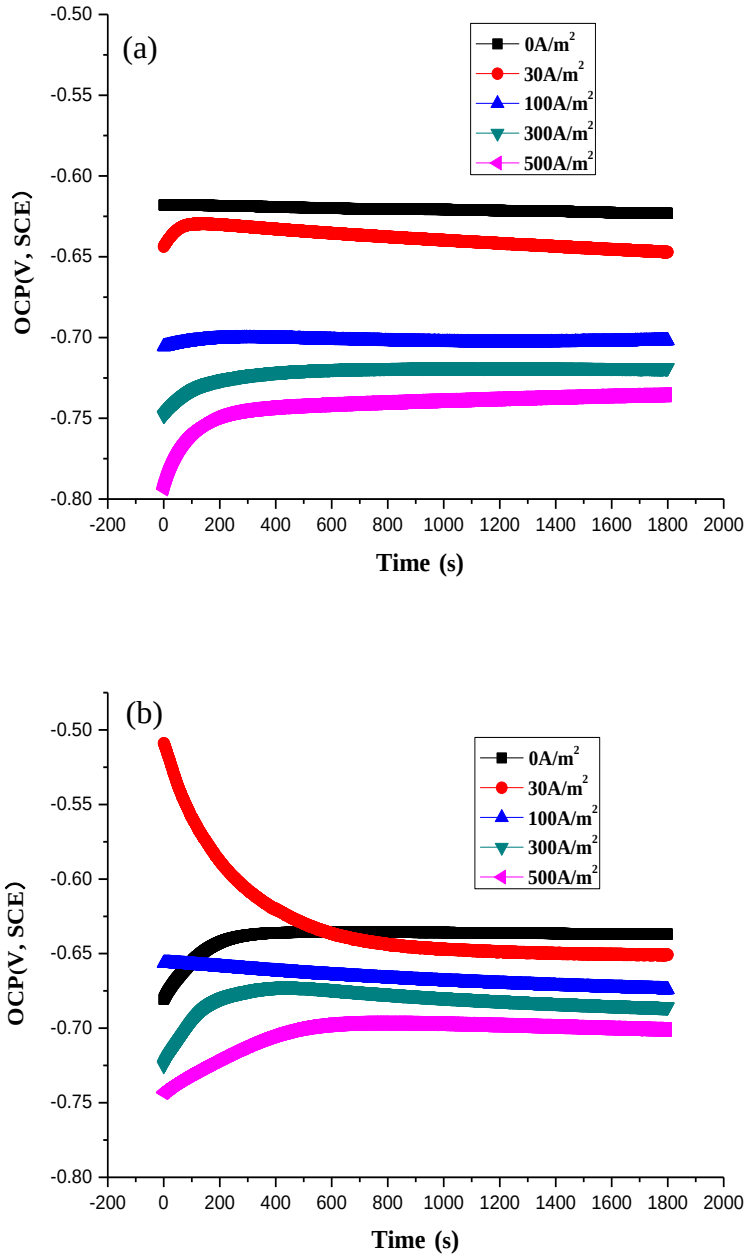

Figure 4. OCP results of X70 coating samples of different defect sizes (a) 0.5×0.5 mm^2, (b) 2×2 mm^2 under AC interference with various current densities

This conclusion is consistent with the previous research. Jiang et al. [5] found that with the increase of AC interference, the OCP of the Q235 steel was shifted negatively and the passivity of the

steel was degraded. Li et al. [9] pointed out that the application of an increasing current density of AC signal shifted the OCP of X70 steel negatively in a simulated marine soil solution. Fu and Cheng [14] studied the effects of AC on corrosion of a coated pipeline steel in carbonate/bicarbonate solution. They found that an application of AC resulted in a negative shift of OCP. Furthermore, under the same level of AC interference, the electrochemical activity of the coated steel with small defects was greater and pitting was more likely to occur. Yang et al. [29] investigated that the OCP of X70 steel samples and corrosion rate increased with the rise of AC density.

3.3 EIS analysis

Fig. 5 shows the EIS results of X70 steel epoxy coating samples with 0.5×0.5 mm^2 defect area at various AC densities. From Fig. 5(a), there are two time constants in the EIS plots under different current densities. In the EIS plots, the impedance of the high-frequency region characterizes the coating itself, and the impedance of the low-frequency region reflects the electrochemical information of the coating/substrate surface. The high-frequency capacitive arcs, which characterize the properties of the coatings, are significantly smaller than the low-frequency capacitive arcs that characterize the corrosion reaction of the iron/coating interface. It is a typical EIS characteristic of defective coatings. The low-frequency capacitance arc is the largest if no AC interference is applied. When the applied AC density increased to 30 A/m^2, the low-frequency capacitance arc slightly reduced. When the AC density increased to 100 A/m^2, the Warburg impedance appeared in the low frequency part. It was a straight line with a slope of about 45°, which indicated that the corrosive medium had penetrated into the interface of the coating/substrate. The reason for the appearance of the low-frequency diffusion tail might be that the corrosion reaction was controlled by the oxidation-reduction diffusion process, such that the semicircular arc, which represents the characteristic of the interface corrosion reaction, is obscured by the Warburg diffusion impedance. In this case, X70 steel substrate in the coating defects had a rust layer. When the AC density is increased to 300 A/m^2, the low-frequency diffusion tail disappeared and becomed a circular arc, which indicated that the corrosion process was controlled by the electrochemical activation of the X70 steel. When the applied AC density continued increasing to 500 A/m^2, the low-frequency capacitive arc further reduced. With the increase of AC density, the low-frequency capacitive arc radius decreased gradually, which indicated that the corrosion resistance decreased. The radius of the low frequency capacitance arc represented the size of the polarization resistance, which was usually inversely proportional to the corrosion rate. Therefore, with the increase of alternating current density, the corrosion rate of coating defects gradually increased. Fig. 5(b) shows that with the application of AC interference increased, the coating impedance gradually reduced. The results revealed that the AC interference made the delamination of the coating worse, which increased X70 exposed steel area at coating defects The corrosion reaction of the X70 steel under the coating film was accelerated.

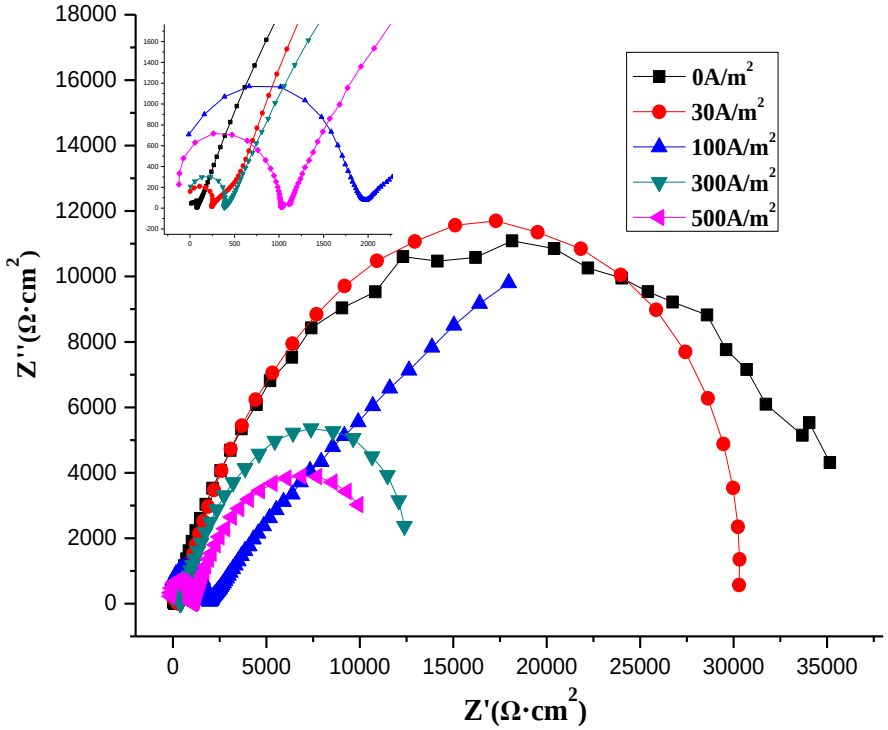

(a) Nyquist

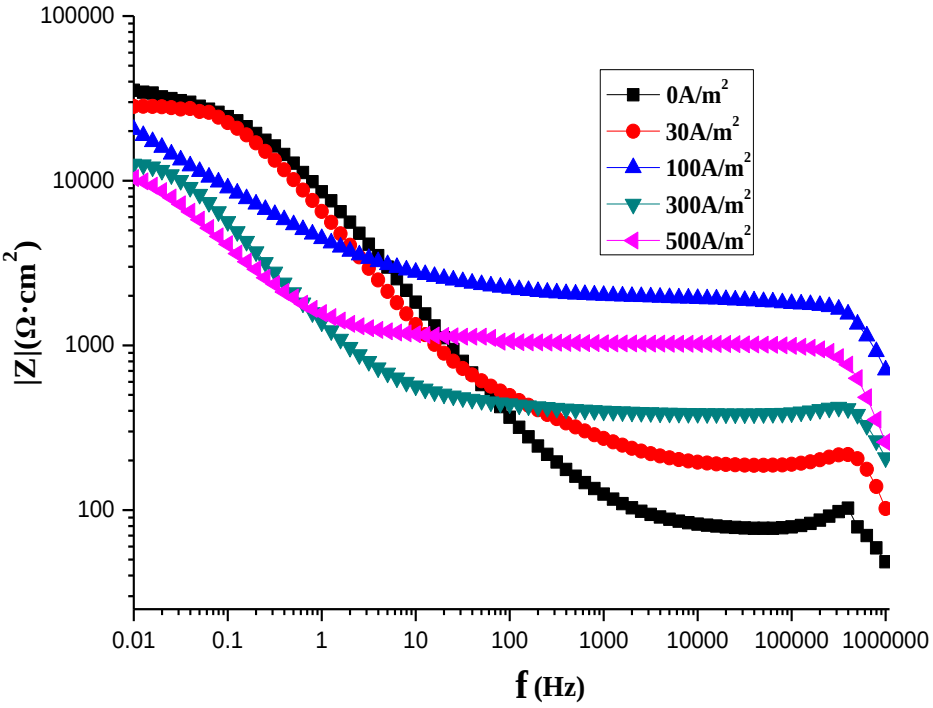

(b) Bode

Figure 5. EIS results of X70 steel coating samples of a 0.5×0.5 mm^2 defect under AC interference with various current densities

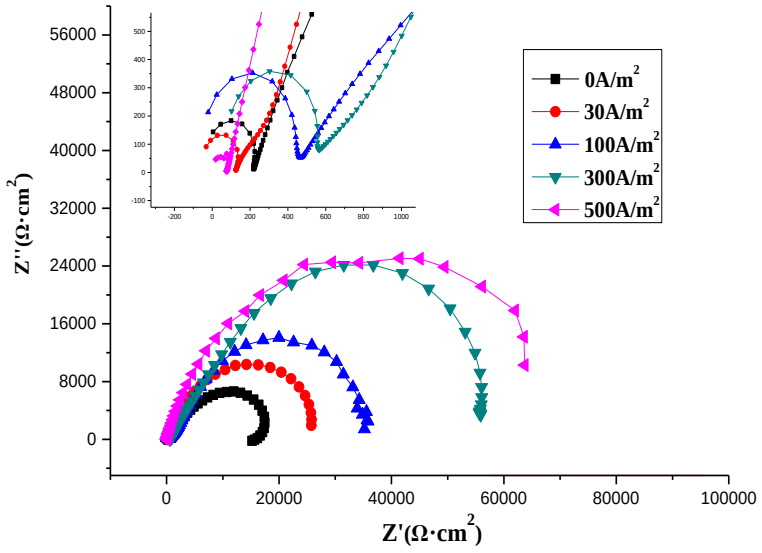

(a) Nyquist

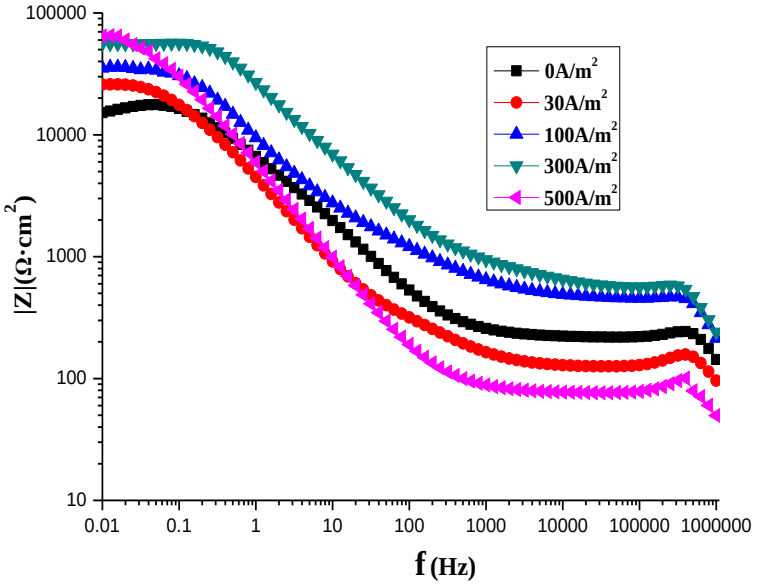

(b) Bode

Figure 6. EIS results of X70 steel coating samples of a 2×2 mm^2 defect under AC interference with various current densities

Fig. 6 shows the EIS results of X70 steel epoxy coating with a 2×2 mm^2 defect area at different AC densities. It can be seen from Fig. 6(a) that when the defect area is large, there are two capacitive arcs in the EIS plots under AC interference at all current densities. When the AC interference was not applied, a small inductive arc appeared at the low frequency side, possibly because the corrosion product was removed from the electrode surface. After applying the AC interference, the low-

frequency inductance arc disappeared, and only the capacitive arc was found. The low-side capacitive arcing expands as the AC density increased. EIS plots have been shown to be an electrochemical process associated with corrosion reaction and deposition of corrosion products in the presence of large surface defects [30]. From Fig. 6(b), we can see that the impedance of the coating increases with the increase of the AC density. This phenomenon is called "self-repairing" [31]. It is because under the AC interference, the anodic dissolution and cathodic reduction of the steel produce a large amount of corrosion products, blocking the pinhole defects. As barriers, corrosion products resist the penetration of corrosive media, causing the coating resistance increasing. With the increase of AC density, this "self-repair" phenomenon is more evident. The corrosion morphology observation shows that the higher of the AC density, the more corrosion products.

The above EIS results can be fitted by the equivalent circuit in Fig. 7. X70 steel coating samples of a 0.5×0.5 mm^2 defect in the application of AC density of 100 A/m^2, the equivalent circuit is shown in Fig. 7(a), the EIS under other AC interference with various current densities can be fitted by the equivalent circuit in Fig. 7(b). Where Rs is the solution resistance, Rc and Qc are the coating resistance and capacitance, respectively. Q_{d1} and Rt are the electric double layer capacitance and the electrochemical reaction resistance of the iron/coating interface, respectively. Z_W is the Warburg impedance. The fitting equivalent circuits are consistent with other researchers [32,33]. Poelman et al. [34] pointed out that the electric double layer capacitance C_{d1} and charge transfer resistance Rt are closely related to the delamination of the coating, the increase of electric double layer capacitance means that the coating delamination area increases. Therefore, the delamination area of the coating can be calculated by the following equations [35].

$$A_d=C_{d1}/C^0_{d1} \quad (1)$$

Among them, C^0_{d1} is a certain area of bare steel electric double layer capacitors. This formula is corrected for the coating with defects to give the equation (2). It can be seen, the same defect area, the size of the electric double layer capacitance is proportional to the coating delamination area.

$$A_d \propto C_{d1}/C^0_{d1} \quad (2)$$

Because the capacitance is not the ideal capacitance in the actual situation, the constant phase angle Q is used instead of the capacitance C in the EIS fitting, which can reflect the electrochemical information of the iron/coating system under the stray current.

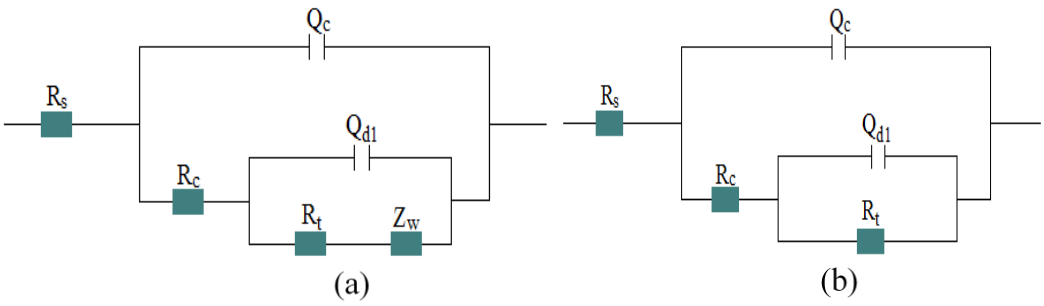

Figure 7. Equivalent Circuit of EIS results

According to the electric double-layer capacitance of the fitting circuit, From Fig. 8, which is the double-layer constant phase angle of the two defects under different AC density. It can be seen from the figure, the coating defect area is 0.5×0.5 mm^2, when the AC density from 0 A/m^2 increased to 30 A/m^2, the normal phase angle Q_{d1} significantly increased, indicating that the coating has obvious delamination. As AC density continues to grow, the magnitude of Q_{d1} is small, indicating that there is a critical current density. When the AC density exceeds this critical value, the delamination area will not continue to increase. When the defect area is 2×2 mm^2, the value of the constant phase angle does not change much, which indicates that the stray current has little effect on the delamination of the large defect coating. Chong et al. [36] showed that the size of the defect existing in coating affected the corrosion behavior of a coated steel significantly because the degree of difficulty in the accumulation of corrosion products at the defect was different.

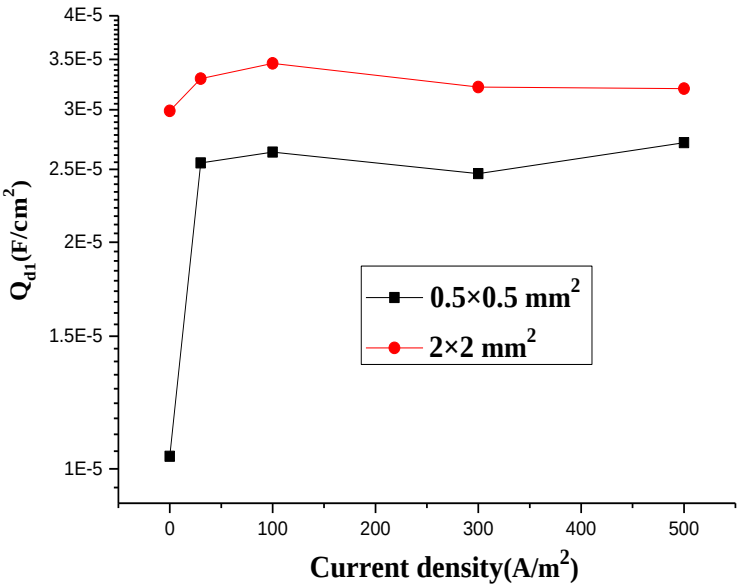

Figure 8. Q_{d1} of samples with different defect sizes under AC interference with various current densities

3.4 Corrosion morphology analysis

Fig. 9 and Fig. 10 are the corrosion morphology of X70 steel epoxy coating samples with different defect under various AC interference. Fig. 11 shows the delamination area of samples with the various sizes under AC interference with various current densities. When the coating defect area is 0.5×0.5 mm^2, the AC density increases from 0 A/m^2 to 30 A/m^2, and the delamination area increases significantly. Thereafter, as the current density increases, the delamination area remains essentially constant, indicating the presence of a delamination critical current density, When the AC density is less than the critical current density, the delamination area increases with the increase of the AC density. When the current density is greater than this critical current density, with the increase of the AC density, the delamination area at coating defect is basically the same. Because the accumulation of corrosion products, defective pores are blocked, and the cathode and anode regions are difficult to

exchange electronically. At the same time, the oxygen content in the solution decreased, resulting in AC interference on the role of coating delamination is significantly reduced. Cao [37] reported that the other experimental conditions were kept constant, the delamination area of the coating increases with the increase of the current density, and then remains unchanged, indicating that the stray DC has a critical current density on the delamination destruction of the coated buried pipeline. Obviously, our conclusion is similar with Cao's work [37].

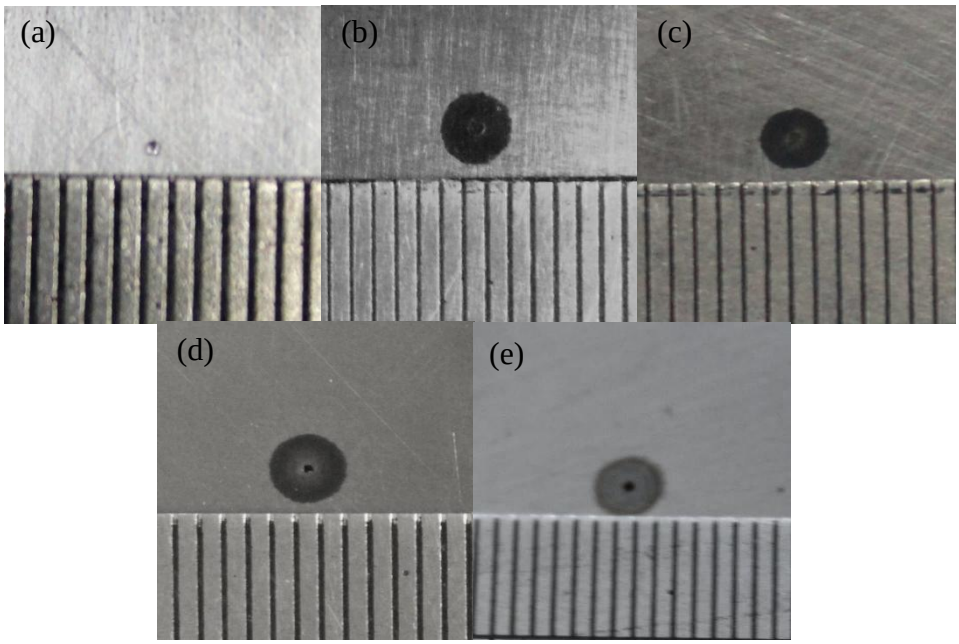

Figure 9. Macroscopic corrosion morphologies of X70 coating samples with a 0.5×0.5 mm^2 defect under AC interference with various current densities (a) 0 A/m^2, (b) 30 A/m^2, (c) 100 A/m^2, (d) 300 A/m^2, (e) 500 A/m^2

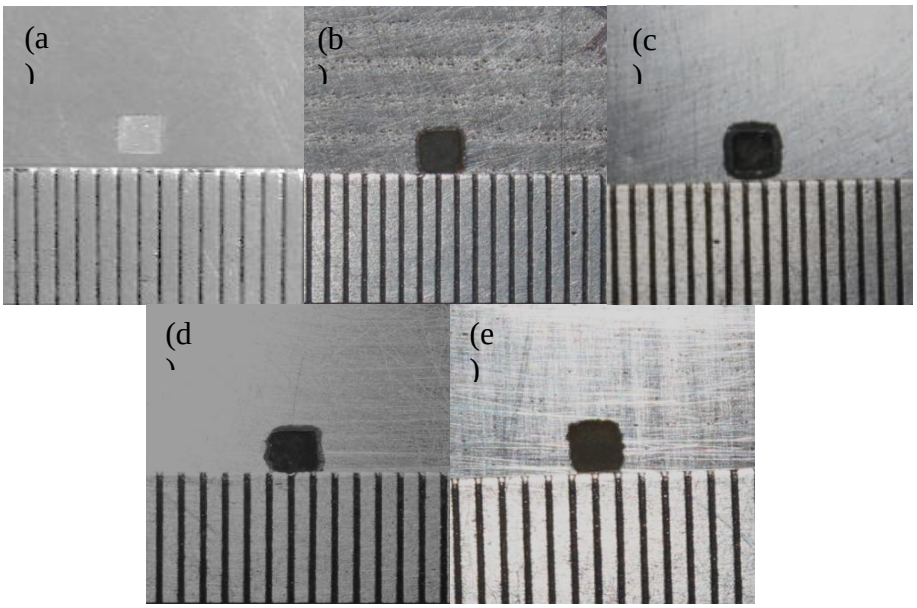

Figure 10. Macroscopic corrosion morphologies of X70 coating samples with a 2×2 mm^2 defect under AC interference with various current densities (a) 0 A/m^2, (b) 30 A/m^2, (c) 100 A/m^2, (d) 300 A/m^2, (e) 500 A/m^2

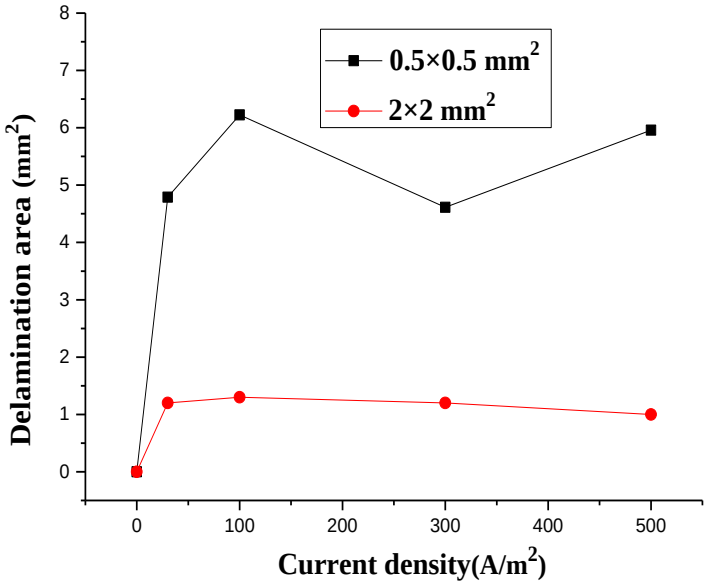

Figure 11. Delamination area of samples with different defect sizes under AC interference with various current densities

At the same AC density, the delamination area of the small defect coating is larger than that of the large defect coating. When the defect area is small, the exposed X70 steel is small, and the defect hole is easily covered by the generated corrosion products. The Fe^{2+} in the corrosion products can react with O_2 to oxidize, and consume the oxygen content at the coating defects. Also, the corrosion product film hinders the permeation of oxygen into the fresh steel under the film of the corrosion product, resulting in the defective center region as an oxygen-depleted region. However, oxygen can diffuse from the edge of the corrosion product film to the edge region of the defect such that the edge region of the defect is an oxygen-enriched region, thus forming separate anode and cathode regions [38,39]. The anodic dissolution of the steel is accelerated due to the lower pH. The pH value of the cathode area is higher, OH^- makes the coating adhesion decreased, the coating saponification reaction and loss of viscosity, leading to coating cathodic delamination [40,41]. When the defect area is 2×2 mm^2, the delamination area is relatively small even if under the AC interference, Because of the large defect area, the corrosion product accumulation at the defect is not as good as that of the small defect coating, and no significant oxygen-deficient and oxygen-deficient regions are formed at the defect center and edge of the defect. Zhang [42] pointed out that the coating system with a smaller damage area has a higher cathode migration rate than a coating system with a large damage by the wire beam electrode (WBE) technique, indicating that the failure rate of the coating with a smaller defect is faster than that of the larger defect. Ding and Fan [43] studied that the smaller of the coated pipeline with damage area, the larger voltage signal value influenced by AC interference, which could lead to the greater effect on the coating delamination. It is clear that our research results are highly consistent with other researchers [36,37,42,43].

4. CONCLUSIONS

The following conclusions can be made based on the results presented in this paper.

(a) The stray current was unevenly distributed on the surface of buried steel pipelines. The current density at the defect edge was higher than that at the defect center and inner surface. It implies that the defect edge possibly suffers from a severe corrosion. It is capable to trigger coating delamination.

(b) The electrochemical behavior at coating defects was influenced by the defect size. When the coating defect was small, the coating resistance decreases with the increase of the AC density, which indicated that the area of exposed X70 steel increases and AC interference accelerated the delamination of the coating. When the coating defect area was large, the impedance of the coating increased with the increase of the AC density. This "self-repairing" phenomenon was caused by the anodic dissolution and cathodic reduction of the steel under AC interference, resulting in a significant amount of corrosion products, as a barrier layer, making the coating resistance increased.

(c) Under the stray AC interference, the coating defect area affected the coating delamination. In the same size defect area, the stray current density increases from 0 A/m^2 to 30 A/m^2 and the delamination area increased significantly. Then, with the growth of the current density, the delamination area remained unchanged, indicating the existence of the critical delamination current density around 30 A/m^2.

(d) At the same stray current density, the small coating defect introduced a larger coating delamination. Therefore, in the stray current conditions for coating defects detection should pay attention to this small size coating defects.

ACKNOWLEDGEMENTS
The authors appreciate the financial supports from National Natural Science Foundation of China Project Number: NSFC 51471011, China Postdoctoral Research Foundation, and Beijing Postdoctoral Science Foundation.

References

1. A. L. Cao, Q. J. Zhu, S. T. Zhang, B. R. Hou, *Anti-Corros. Methods Mater*. 57 (2010) 234.
2. S. R. Allahkaram, M. Isakhani-Zakaria, M. Derakhshani, M. Samadian, H. S. Rasaey and A. Razmjoo, *J. Nat. Gas Sci. Eng.* 26 (2015) 453.
3. L. Bertolini, M. Carsana and P. Pedeferri, *Corros. Sci*. 49 (2007) 1056.
4. A. O. S. Solgaard, M. Carsana, M. R. Geiker, A. Küter and L. Bertolini, *Corros. Sci*. 74 (2013) 1.
5. Z. T. Jiang, Y. X. Du, M. X. Lu, Y. N. Zhang, D. Z. Tang, L. Dong, *Corros. Sci.* 81 (2014) 1.
6. C. Wen, J. B. Li, S. L. Wang, Y. Yang, *J. Nat. Gas Sci. Eng*. 27 (2015) 1555.
7. M. Zhu, C. W. Du, X. G. Li, Z. Y. Liu, S. R. Wang, *Electrochim. Acta*. 117 (2014) 351.
8. L. Y. Xu, X. Su, Z. X. Yin, Y. H. Tang, Y. F. Cheng, *Corros. Sci*. 61 (2012) 215.
9. Y. C. Li, C. Xu, R. H. Zhang, Q. Liu, X. H. Wang, Y. C. Chen, *Int. J. Electrochem. Sci*. 12 (2017) 1829.
10. B. Uillemin, R. Oltra, R. Cottis, *Electrochim. Acta*. 27 (2007) 7570.
11. S. Goidanich, L. Lazzari, M. Ormellese, *Corros Sci*, 52 (2010) 491.
12. Y. Li, F. Dawalib, *Corros. Sci*. 28 (2004) 197.

13. A. B. Forero, J. A. C. Ponciano, I. S. Bott, *Mater. Corros*. 63 (2012) 9999.
14. A. Q. Fu, Y. F. Cheng, *Corros. Sci*. 52 (2010) 612.
15. D. Kuang, Y. F. Cheng, *Corros. Sci*. 85 (2014) 304.
16. R. Zhang, P. R. Vairavanathan, S. B. Lalvani, *Corros. Sci*. 50 (2008) 1664.
17. F. Mohammadi, F. F. Eliyan, A. Alfantazi, *Corros. Sci*. 63 (2012) 323.
18. R. W. Bosch, W. F. Bogaerts, *Corros. Sci*. 40 (1998) 323.
19. S. B. Lalvani, X. Lin, *Corros. Sci*. 38 (1996) 1709.
20. S. Goidanich, L. Lazzari, M. Ormellese, M. Pedeferri, *Corrosion'* 2005, NACE, Paper No. 05189.
21. N. W. Khun, G. S. Frankel, *Prog. Org. Coat*. 99 (2016) 55.
22. S. Adhikari, K. A. Unocic, Y. Zhai, G. S. Frankel, J. Zimmerman, W. Fristad, *Electrochim. Acta*. 56 (2011) 1912.
23. H. Bi, J. Sykes, *Corros. Sci*. 53 (2011) 3416.
24. S. H. Lee, W. K. Oh, J. G. Kim, *Prog. Org. Coat*. 76 (2013) 778.
25. D. A. Worsley, D.Williams, J. S. G. Ling, *Corros. Sci*. 43 (2001) 2335.
26. S. Shreepathi, *Prog. Org. Coat*. 90 (2016) 438.
27. S. Walkner, A. W. Hassel, *Electrochim. Acta*. 131 (2014) 130.
28. V. Guillaumin, D. Landolt, *Corros. Sci*.44 (2002) 179.
29. Y. Yang, Z. Li, C. Wen, *Acta Metall. Sin*. 49 (2013) 43.
30. S. H. Lee, W. K. Oh, J. G. Kim, *Prog. Org. Coat*. 76 (2013) 784.
31. E. D. Schachinger, R. Braidt, B. Straub, A. W. Hassel, *Corros. Sci*. 96 (2015) 6.
32. X. Q. Xue, J. F. Lu, *Int. J. Electrochem. Sci*. 12 (2017) 3179.
33. J. W. Wu, Y. H. Cui, W. Yuan, J. S. Wu, Z. H. Li, *Int. J. Electrochem. Sci*. 10 (2015) 9919.
34. M. Poelman, M. G. Olivier, N. Gayarre, J. P. Petitjean, *Prog. Org. Coat*. 54 (2005) 55.
35. H. J. Wang, J. Wang, W. Wang, W. Zhang, *J. Ocean Univ. China*. 14 (2015) 269.
36. C. Zhong, X. Tang, Y. F. Cheng, *Electrochim. Acta*. 53 (2008) 4740.
37. A. Lin Cao, Chongqing University. *China*. (2010).
38. H. Bi, J. Sykes, *Prog. Org. Coat*. 90 (2016) 114.
39. P.A. Sørensen, S. Kiil, K. Dam-Johansen, C.E. Weinell, *Prog. Org. Coat*. 64 (2009) 142.
40. N. W. Khun, G. S. Frankel, *Corros. Sci*. 67 (2013) 152.
41. J. Wielant, R. Ponser, G. Grundmeier, H. Terryn, *Corros. Sci*. 51 (2009) 1664.
42. Y. Zhang, Ocean Univ. China. (2015).
43. Q. M. Ding and Y. M. Fan, *Int. J. Corrosion*. 2016 (2016) 1.